Aspects of static and dynamic magnetic anisotropy in $Ni_{81}Fe_{19}$-NiO films

Jeffrey McCord,* Rainer Kaltofen, Thomas Gemming, Ruben Hühne, and Ludwig Schultz
Leibniz Institute for Solid State and Materials Research IFW Dresden, Postfach 270116, 01171 Dresden, Germany
(Received 17 October 2006; revised manuscript received 5 January 2007; published 19 April 2007)

The strength of the unidirectional, uniaxial, cubic, and dynamic rotatable anisotropy field together with the effective damping parameter in polycrystalline $Ni_{81}Fe_{19}$/NiO ferromagnet and/or antiferromagnet systems is studied as a function of NiO thickness and thermal history. A partial transformation of antiferromagnetically induced combined uniaxial and cubic anisotropy to undirectional anisotropy with increasing NiO thickness is confirmed by hysteresis loop modeling. Independent of the occurrence of exchange bias, the overall exchange anisotropy is constant over a wide range of NiO thickness. A reduction of exchange bias with initial annealing is due to a transformation from a fixed to a rotatable antiferromagnetic spin structure, manifesting itself in the appearance of rotatable anisotropy. With annealing at the interface a $Ni_xFe_yO_z$ layer is formed that changes the interfacial coupling, leading to an additionally enhanced rotatable anisotropy and spin-wave damping. The data imply that the spin structure inside the antiferromagnetic layer is responsible for exchange bias and the dominating contribution to coercivity, the interfacial structure for the overall coupling. The chemical interface structure and the thermomagnetic history are relevant, and have to be taken into account, comparing experimental data with theoretical models of exchange coupling.

DOI: 10.1103/PhysRevB.75.134418 PACS number(s): 75.40.Gb, 75.70.−i, 76.50.+g

I. INTRODUCTION

Exchange-coupled magnetic thin films consisting of an antiferromagnetic (AF) and an adjacent ferromagnetic (F) layer are an essential part of today's spin electronic applications, as they are used as a part of magnetoresistive devices in current magnetic recording technology or proposed magnetic random access memory cells. Mostly, the technological purpose of using F/AF systems is the magnetic stabilization of the F layer relative to applied external magnetic fields. The stabilization of magnetization is based on the phenomenon of exchange bias, which manifests itself in a magnetic loop shift or exchange bias field[1] $H_{EB,AF}$ along a preferred direction (see Refs. 2–4 for reviews of exchange bias). The unidirectional anisotropy can be set either during film deposition or by field cooling, both in an applied magnetic field. Various models have been developed to describe the exchange bias field in reasonable agreement with experimentally obtained data.[5–11] Recent experiments[12,13] provide direct experimental evidence for the existence of uncompensated interfacial spins being responsible for the unidirectional anisotropy.

In addition to the unidirectional anisotropy, higher-order anisotropy terms are detected in polycrystalline and epitaxial F/AF systems.[14–16] Moreover, in polycrystalline thin film systems an increase of coercivity $H_{c,EA}$ with the occurrence of exchange bias is observed. Several mechanisms have been proposed to account for the change in coercivity. First, irreversible and time-dependent magnetization processes due to thermally activated switching events in a viscous AF layer[17–19] presumably lead to the increase in hysteresis loss. Other experiments suggest the formation of interfacial magnetic spins[20,21] coupled to a static AF spin structure as being responsible for the increase in coercivity. Despite all the experimental and theoretical investigations focusing on the actual spin arrangement at the AF interface, the mechanism controlling the final spin structure at the interface is still not known. In principle, several phenomena might be contributing collectively.

Further insight into the nature of the F/AF interaction can be gained from the magnetization dynamics of exchange-biased thin films. In comparison to single-layer F thin films, F/AF structures display an increase in ferromagnetic resonance linewidth or effective spin-wave damping α_{eff},[22–25] which also depends on temperature and AF layer thickness. The results of the experiments are interpreted in terms of an inhomogeneous spin structure due to an inhomogeneous magnetization distribution within the F layer or a magnetically rough F/AF interface.[26] The latter assumption is in agreement with an inhomogeneous AF grain or domain structure, hence resulting in a variation of the local magnetic coupling field. Additional dynamic effects from thermal instabilities of the AF below the blocking temperature of the AF structure are reported.[25,27] Furthermore, isotropic ferromagnetic resonance frequency shifts are observed in ferromagnetic resonance experiments[22] and related to a rotatable anisotropy field[28] H_{rot} that arises from thermally activated switching of AF grains[8] or from changes in the antiferromagnetic domain structure. As stated before, these irreversible changes in the AF domain structure should also be visible in an increase of coercivity. A detailed introduction to the aspects of rotatable anisotropy and the related anisotropy enhancement can be found in Ref. 8.

In this paper the static and dynamic magnetic properties in polycrystalline $Ni_{81}Fe_{19}$-NiO films with varying AF layer thickness (thus with altered anisotropy energy of the AF layer) were investigated. Furthermore, as-deposited structures were compared to subsequently field-annealed samples to separate effects from the F/AF interface and the internal AF domain structure.

II. EXPERIMENT

$Si/SiO_2/Ta(4\ nm)/Ni_{81}Fe_{19}(30\ nm)/NiO(0–50\ nm)$ structures were prepared by magnetron sputtering in a mul-

tisource high-vacuum sputter system with a base pressure below 2×10^{-7} mbar at an Ar pressure of 8×10^{-4} mbar. rf mode was used for the NiO and the Ta layer deposition, and dc mode for the other metallic layers. The Ta seed layer ensured a ⟨111⟩ texture for the growth of the polycrystalline films. The deposition rate for the NiO layer was 1.7 nm/min. The F uniaxial anisotropy axis and the initial exchange bias direction were set in an applied magnetic in-plane field of $H_{\mathrm{dep}}\approx250$ Oe during deposition of the films. In addition, the films were vacuum annealed at 250 °C in an applied field of $H_{\mathrm{ext}}=10$ kOe with varying time up to 1 h.

The texture of the films was characterized by x-ray pole figure measurements using a standard four-axis goniometer and Cu $K\alpha$ radiation. Further microstructural analysis of selected as-deposited and annealed samples was performed by high-resolution analytical scanning transmission electron microscopy (STEM) experiments with electron energy-loss spectroscopy (EELS). Grain size and structure, as well as the element composition across the F/AF interface, were extracted from the TEM data.

Regular inductive magnetometry with an inductive loop tracer at an operating frequency of 10 Hz in combination with dynamic magnetization response measurements by pulsed inductive micrometer magnetometry[29] was used to investigate the exchange anisotropies relevant for the understanding of the exchange coupling.[25] From the hysteresis loop measurements along the easy axis of magnetization the exchange bias field $H_{\mathrm{EB,AF}}$ was derived using the simple relation

$$\vec{H}_{\mathrm{EB,AF}}=-\frac{1}{2}(\vec{H}_{c1}+\vec{H}_{c2}), \tag{1}$$

where H_{c1} and H_{c2} are the coercivity field values for the downward and upward loop branches, respectively. This is only valid under the assumption of a symmetric hysteresis behavior.

A more correct method to probe the static exchange bias field is by the measurement of the magnetic response along the magnetic hard axis (HA). The effective anisotropy field $\vec{H}_{k,\mathrm{F+AF}}$ acting on the F layer can be derived by extrapolating the HA loop from zero field to saturation. In the simplest model $\vec{H}_{k,\mathrm{F+AF}}$ is composed by the ferromagnetic uniaxial anisotropy field $\vec{H}_{k,\mathrm{F}}$ and the unidirectional field $\vec{H}_{\mathrm{EB,AF}}$. For our analysis we introduced an additional term, an AF-induced anisotropy field $\vec{H}_{k,\mathrm{AF}}$. The total anisotropy field acting on the F layer is then

$$\vec{H}_{k,\mathrm{F+AF}}=\underbrace{\vec{H}_{k,\mathrm{F}}}_{\mathrm{F}}+\underbrace{\vec{H}_{\mathrm{EB,AF}}+\vec{H}_{k,\mathrm{AF}}}_{\mathrm{AF}}=\vec{H}_{k,\mathrm{F}}+\vec{H}_{\mathrm{stat,AF}}, \tag{2}$$

where the total size of the AF-induced static anisotropy field is summarized in $\vec{H}_{\mathrm{stat,AF}}$.

In addition, the anisotropy can be derived from the dynamic magnetic response at the nanosecond time scale, thus avoiding thermally activated switching events in the AF layer.[25] Measuring the dependence of f_{res} on a varying, additionally applied external bias field $\vec{H}_{\mathrm{bias}}$, a linear dependency in accordance with the simplified Kittel formula[30]

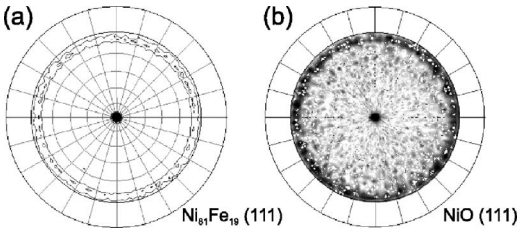

FIG. 1. (a) $Ni_{81}Fe_{19}$ (111) and (b) NiO (111) pole figures from a $Ni_{81}Fe_{19}$ (30 nm)/NiO (50 nm) bilayer structure.

$$f_{\mathrm{res}}^2=\left(\frac{\gamma\mu_0}{2\pi}\right)^2 M_{\mathrm{s}}(\vec{H}_{\mathrm{dyn,F+AF}}+\vec{H}_{\mathrm{bias}}) \tag{3}$$

is expected. The important magnetic parameter that was extracted from these measurements was the value for the effective dynamic anisotropy field $\vec{H}_{\mathrm{dyn,F+AF}}$, which summarizes the anisotropy field $\vec{H}_{k,\mathrm{F}}$ of the FM layer, and additional AF-induced contributions including a direction-independent or rotatable anisotropy field $\vec{H}_{\mathrm{rot,AF}}$:[25,32]

$$\vec{H}_{\mathrm{dyn,F+AF}}=\underbrace{\vec{H}_{k\ \mathrm{F}}}_{\mathrm{F}}+\underbrace{\vec{H}_{\mathrm{EB,AF}}+\vec{H}_{k,\mathrm{AF}}+\vec{H}_{\mathrm{rot,AF}}}_{\mathrm{AF}}=\vec{H}_{k,\mathrm{F}}+\vec{H}_{\mathrm{dyn,AF}}. \tag{4}$$

Equation (4) differs from Eq. (2) only by the term $\vec{H}_{\mathrm{rot,AF}}$. The AF contribution to the dynamic anisotropy field is summarized in $\vec{H}_{\mathrm{dyn,AF}}$. All three methods are applied in this work and the results are compared.

Supplementary to f_{res}, the effective magnetic damping parameter α_{eff} was extracted from the dynamic measurements. It was derived from the exponential decay time[31] τ of the resonant magnetic response using

$$\alpha_{\mathrm{eff}}=\frac{2}{\tau\gamma\mu_0 M_s}. \tag{5}$$

III. MICROSTRUCTURAL ANALYSIS

The $Ni_{81}Fe_{19}$ and NiO pole figures for the (111) axis, obtained on a $Ni_{81}Fe_{19}$(30 nm)/NiO(50 nm) bilayer, are displayed in Fig. 1. A distinct (111) fiber texture was found for both magnetic layers, the $Ni_{81}Fe_{19}$ and the NiO. No sign of in-plane texture was detected.

STEM dark-field images from a F/AF bilayer with $t_{\mathrm{NiO}}=50$ nm are displayed in Fig. 2. The grain structure is columnar across the F/AF interface, both for the as-deposited state [Fig. 2(a)] and after an 1 h annealing at 250 °C [Fig. 2(b)]. No significant change in the columnar grain structure occurs with annealing. An average grain diameter of approximately 15 nm is derived from the TEM images. EELS line scans showing the spatial distribution of O, Ni, and Fe across the AF interface for an as-deposited and a 1 h annealed sample are shown in Fig. 3. For the as-deposited state [Fig. 3(a)] a

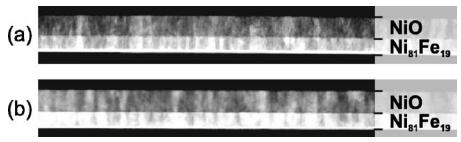

FIG. 2. Dark-field STEM images of an as-deposited (a) and annealed (b) NiO (50 nm)/$Ni_{81}Fe_{19}$ (30 nm) structure (annealing time t_{ann}=1 h).

slight enrichment of Ni concentration in the $Ni_{81}Fe_{19}$ layer and depletion in the NiO layer is observed at the F/AF interface. Whereas in the as-deposited state only these minor effects are found, with annealing [Fig. 3(b)] a more pronounced increase of Fe and concurrent depletion in Ni concentration at the F/AF interface is detected. The element distribution together with the corresponding EEL spectra reveal the generation of a $Ni_xFe_yO_z$ layer at the interface after thermal treatment. The interfacial layer has a thickness of approximately 1–2 nm. An effective transformation from a magnetic bilayer to a magnetic trilayer structure takes place.

IV. MAGNETIC ANALYSIS AND DISCUSSION

A. As-deposited films

Example hysteresis loops along the magnetic easy axis (EA) and HA for different NiO thicknesses are displayed in Fig. 4. For the thinnest NiO layer [t_{NiO}=5.0 nm, Fig. 4(a)] an increase in coercivity along the EA (single-layer coercivity $H_{c,F}$=1.5 Oe) and a two-step magnetization loop along the HA [Fig. 4(c)] are seen. With increasing AF layer thickness [Fig. 4(b)] magnetic loop shift is observed along the EA, indicating exchange bias. The EA coercivity has decreased relative to the sample with t_{NiO}=5 nm, but is still higher than for the pure F layer. Only a slight hint of a two-step magnetization process is visible in the corresponding nearly linear HA loop. As indicated, the total AF-induced anisotropy field, $H_{stat,AF}$, as derived from the HA curves, is much higher than expected from $H_{EB,AF}$, alone.

The discrepancy between the statically obtained parameters $H_{EB,AF}$ and $H_{stat,AF}$ can in principle be described by the introduction of higher-order anisotropy terms[15] or a cubic anisotropy term.[16] As shown in Ref. 16 the occurrence and

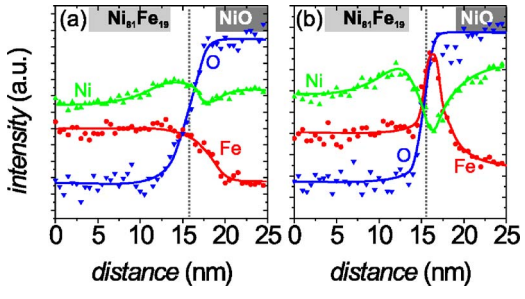

FIG. 3. (Color online) EELS line scans perpendicular to the F/AF interface for the as-deposited (a) and annealed (b) NiO (50 nm)/$Ni_{81}Fe_{19}$ (30 nm) sample. The annealing time t_{anneal} was 1 h. The presumed position of the NiO/$Ni_{81}Fe_{19}$ interface is indicated by a dotted line.

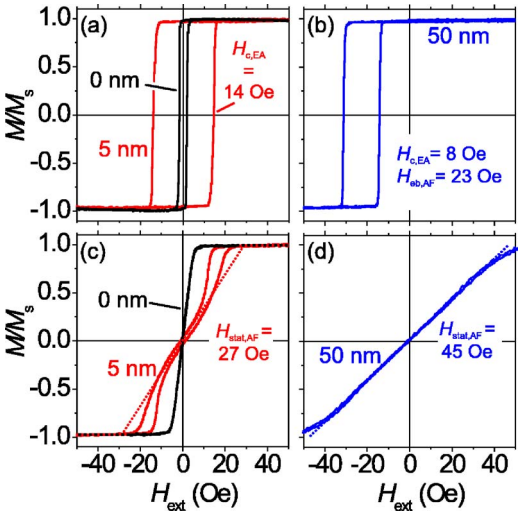

FIG. 4. (Color online) Hysteresis loops along the easy axis of (a) a single $Ni_{81}Fe_{19}$ (30 nm) layer and $Ni_{81}Fe_{19}$ (30 nm)/NiO bilayers with a NiO thickness of 5 nm and (b) of 50 nm are shown. The exchange bias field $H_{EB,AF}$ and the coercivity values $H_{c,EA}$ are indicated. The hard axis loops for the same samples are displayed in (c) and (d), respectively. The values of $H_{stat,AF}$ for the bilayer samples, obtained by extrapolation as indicated by the dotted lines, are shown. Note the close compliance of the linear line with the HA loop in (d).

direction of additional anisotropies is not affected by NiO crystallinity, but only by the interfacial spin structure. Furthermore, in our analysis, no sign of in-plane texture was found (Fig. 1). Therefore, direct effects from the crystallinity of the NiO layer on the in-plane distribution of AF-induced anisotropy can be excluded. A two-step magnetization reversal was also reported in Ref. 14. There, the S-shaped HA loop was interpreted as an AF-induced uniaxial-like anisotropy, existing only at low fields and "unsnapping" at higher magnetic fields.

To exemplarily simulate the shape of the hysteresis loops, the simultaneous occurrence of AF-induced interfacial unidirectional and combined uniaxial and cubic anisotropy terms is assumed. (Similar loop shapes were obtained under the assumption of a critical angle of twist between F and AF magnetization, as proposed by Stiles and McMichael,[32] similar to the simulations used in Ref. 14.) For the shown data, the ratio between unidirectional, uniaxial, and cubic anisotropy contribution is varied. A constant interfacial exchange anisotropy J_{AF} is assumed. The amount of coupling leading to exchange bias $f_{EB,AF}$, uniaxial $f_{u,AF}$, and cubic anisotropy $f_{c,AF}$ is kept fixed with $f_{EB,AF}+f_{u,AF}+f_{c,AF}=1$. The AF-induced energy contribution acting on the F layer is then defined as

$$e_{ani,AF} = -f_{EB,AF}J_{AF}\cos(\beta-\alpha) + \frac{1}{2}f_{u,AF}J_{AF}\sin^2(\beta-\alpha) + \frac{1}{4}f_{c,AF}J_{AF}\sin^2(\beta-\alpha)\cos^2(\beta-\alpha), \quad (6)$$

where J_{AF} is the interfacial exchange coupling, α the direc-

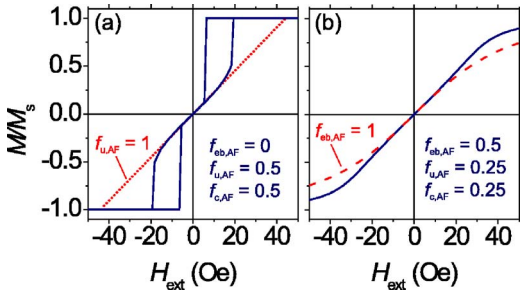

FIG. 5. (Color online) Calculated HA hysteresis loops for a constant J_{AF} with (a) no unidirectional, but equally contributing unidirectional and uniaxial anisotropy terms and (b) a combination of all three acting anisotropy terms. The fractions of unidirectional $f_{EB,AF}$, uniaxial $f_{u,AF}$, and cubic $f_{c,AF}$ anisotropy contributions are indicated (see text for details). The calculated loops for $f_{u,AF}=1$ and $f_{EB,AF}=1$ are added in (a) and (b), respectively.

tion of exchange anisotropy, and β the direction of F magnetization.

The proposed phenomenological model then leads to a total energy density e_{total}

$$e_{total} = -H_{ext}J_s t_F \cos(\varphi - \beta) + \frac{1}{2}K_{u,F}t_F \sin^2(\beta - \theta) + e_{ani,AF}, \tag{7}$$

where the external field H_{ext} aligned under an angle φ, the saturation polarization J_s, and the ferromagnetic layer thickness t_F combine to give the Zeeman energy. $K_{u,F}$ is the uniaxial anisotropy constant of the F layer aligned along θ.

Results for $J_{AF}=10^{-5}$ J/m with $f_{k,AF}=0.5$ and $f_{c,AF}=0.5$, which means without any unidirectional anisotropy, and $f_{EB,AF}=0.5$, $f_{u,AF}=0.25$, and $f_{c,AF}=0.25$ are displayed in Figs. 5(a) and 5(b), respectively. A uniaxial anisotropy of $K_{u,F}=200$ J/m^3 derived from the F single layer is used for the calculations. The calculated reversal for $f_{u,AF}=1$ and $f_{EB,AF}=1$ is added in Figs. 5(a) and 5(b) for comparison. The features of the measured hysteresis loops, the two-step reversal [Fig. 5(a)] and the extended linear regime [Fig. 5(b)] are qualitatively reproduced. As shown, the reversal process can be modeled by the introduction of exchange anisotropy terms of different order assuming just one AF-induced coupling constant J_{AF}. The overall exchange anisotropy $H_{stat,AF}$ can be derived from the slope of the HA loop at $H_{ext}=0$ Oe.

Exemplary dynamic measurement data of the NiO thickness dependence of the effective dynamic anisotropy contributions for the as-deposited films are displayed in Fig. 6. With the addition of the AF layer a frequency shift to higher values relative to the single-layer $Ni_{81}Fe_{19}$ occurs. Despite the differences in magnetic loop shift and coercivity, f_{res}^2 or the effective exchange coupling field $H_{dyn,AF}$ for the thin and the thick NiO layers is equal [Figs. 6(a) and 6(b)], i.e., it is independent of the occurrence of exchange bias. The values of f_{res}^2 at $H_{bias}=0$ Oe are the same for both NiO thicknesses. Deviations in the dynamic response, which become visible from the change of f_{res} with H_{bias}, are shown in Figs. 6(c) and 6(d). With increasing NiO thickness, a horizontal shift in the resonance frequency dependence takes place. This is in

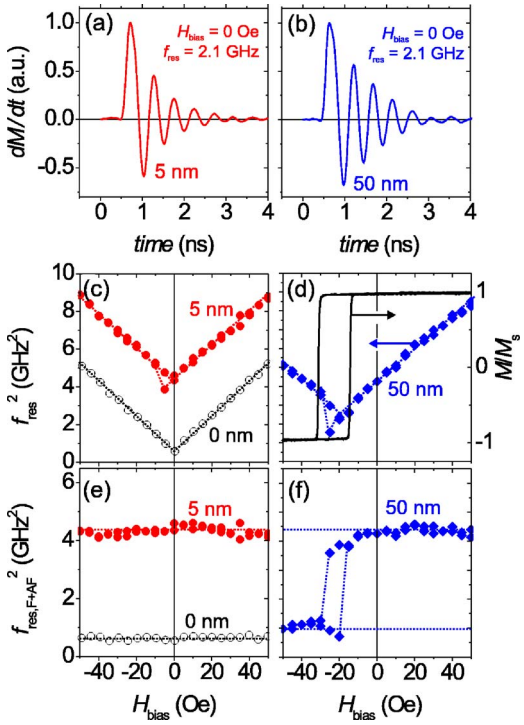

FIG. 6. (Color online) Dynamic response curves at $H_{bias}=0$ Oe for a bilayer with a NiO thickness of (a) 5 and (b) 30 nm. Values of the precessional resonance frequency f_{res} are indicated. (c) f_{res}^2 dependences for $t_{NiO}=0$ and 5 nm. (d) f_{res}^2 for $t_{NiO}=30$ nm with the corresponding EA magnetization curve of Fig. 4. The effective anisotropy field contribution to the precessional frequency $f_{res,F+AF}^2$ vs H_{bias} extracted from (c) and (d) is plotted in (e) and (f), respectively (see text for details).

agreement with the static measurements. The H_{bias} dependence of $H_{dyn,F+AF}$, or more precisely the correlated dependence of $f_{res,F+AF}^2=f_{res}^2-(\gamma\mu_0/2\pi)^2M_sH_{bias}$ [see Eq. (3)], is plotted in Figs. 6(e) and 6(f). Whereas for $t_{NiO}=5$ nm only a resonance shift to higher frequencies is observed, for $t_{NiO}=50$ nm a hysteresislike behavior of the effective coupling field is found. The ostensible decrease of the coercivity in the dynamic measurements reflects the influence of the additional pulse field excitation, resulting in an earlier switching of magnetization.

We interpret the H_{bias} dependence of $f_{res,AF}^2$ as follows. In the case of thin NiO layers, the uncompensated moments of the AF are rotating with the F magnetization,[32,33] because the AF domain or grain anisotropy energy is smaller than the coupling energy between the F and AF layers. With thick NiO layers exchange bias develops, and the drop of $H_{dyn,AF}$ at $H_{bias}<-H_{EB,AF}$ is consequently interpreted as the reduction of coupling field due to the twisting of uncompensated AF spins relative to the F magnetization, which "loosens"[5,33] the pinning of the $Ni_{81}Fe_{19}$ layer magnetization to the NiO layer for fields below $H_{EB,AF}$. The data indicate that with increasing t_{NiO} or AF grain volume a direct transformation of a rotatable to a static spin structure in the AF layer occurs.

A complete overview of the change of the magnetic properties with NiO thickness t_{NiO} is displayed in Fig. 7. The data derived from the EA loops are shown in Fig. 7(a). The coer-

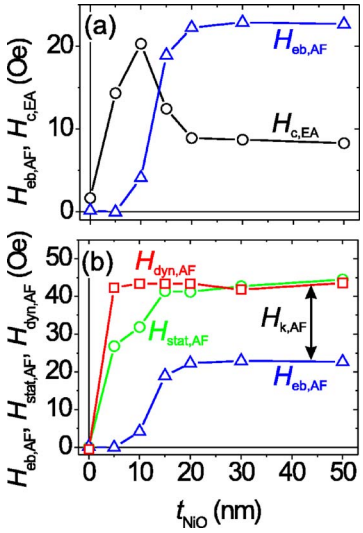

FIG. 7. (Color online) (a) Change of coercivity $H_{c,EA}$ and exchange bias field $H_{EB,AF}$. In (b) $H_{EB,AF}$ as derived from Eq. (1), the measured anisotropy field $H_{stat,AF}$ according to Eq. (2), and the dynamically obtained $H_{dyn,AF}$ as derived from Eq. (4) are compared. The $Ni_{81}Fe_{19}$ anisotropy field $H_{k,F}$ was assumed to be constant for all samples. All data as a function of NiO thickness.

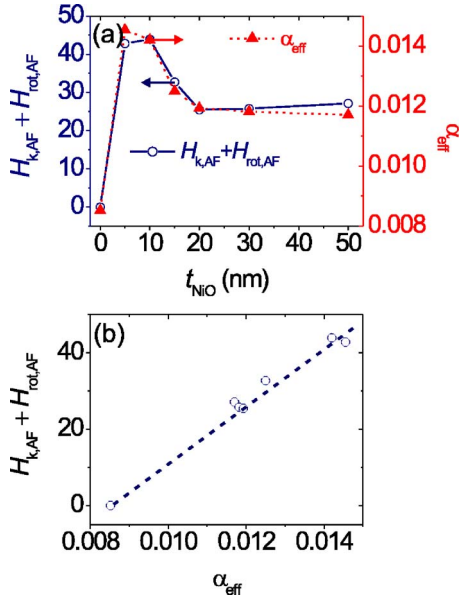

FIG. 8. (Color online) (a) Measured change of the effective damping parameter α_{eff} (▲) together with the change of $H_{k,AF}+H_{rot}$ (○) as a function of NiO thickness. The correlation between α_{eff} and $H_{k,AF}+H_{rot}$ is plotted in (b).

civity field $H_{c,EA}$ peaks around $t_{NiO}=10$ nm and stays almost constant above $t_{NiO}=20$ nm. The maximum of $H_{c,EA}$ is at the onset of exchange bias at $t_{NiO}=15$ nm. As the only parameter varied is the NiO thickness and no difference at the F/AF interface is expected for the investigated bilayers, the increase in coercivity is mainly related to the change in thickness of the AF layer. The difference between $H_{EB,AF}$ and the AF-induced anisotropy fields derived from the HA measurement and from f_{res} is shown in Fig. 7(b). The dynamic data are obtained from analyzing f_{res} at $H_{bias}=0$ Oe, i.e., in a status where the magnetization of the $Ni_{81}Fe_{19}$-layer is parallel to $H_{EB,AF}$, which is the direction of the magnetic field applied during film deposition. With the addition of NiO, even for small thicknesses, where $H_{EB,AF}$ is still zero, a strong exchange field $H_{k,AF}$ is derived from the measurements. With increasing t_{NiO} the AF-induced static anisotropy field $H_{stat,AF}$ remains constant. The dynamically obtained total AF interfacial field $H_{dyn,AF}$ is not changing with t_{NiO} and is equal to $H_{stat,AF}$ above $t_{NiO}=10$ nm. This means that no rotational anisotropy field $H_{rot,AF}$ is detected with thick NiO layers. The precessional frequency shift, observed in the dynamic measurements along the HA, is mostly due to the additional static anisotropy field $H_{k,AF}$ detected for all AF thicknesses. With large AF layer thickness $H_{rot,AF}$ transforms into a more stable AF spin structure, where no difference between $H_{stat,AF}$ and $H_{dyn,AF}$ is visible. The data confirm the proposed gradual transformation of a completely unstable uncompensated spin configuration to a more stable configuration with thicker NiO layers.

The NiO thickness dependence of the damping parameter α_{eff} is plotted in Fig. 8. After a steep increase with $t_{NiO}=5$ nm, it decreases again, but is still higher than in the case of the single $Ni_{81}Fe_{19}$ layer. It follows almost exactly the dependence of the nonunidirectional anisotropy field $H_{k,AF}+H_{rot,AF}$ with t_{NiO}. This observation is expected from models explaining the damping by a two-magnon scattering contribution to the extrinsic damping due to an unstable AF magnetization not contributing to exchange bias. The increased damping of spin waves at the F/AF interface for thin NiO layers is assumed to be due to the dragging of a fraction of AF spins, which correlates with the unstable anisotropy fields $H_{k,AF}+H_{rot,AF}$, by the excited F spins as proposed in Ref. 34.

B. 1-h-annealed films

EA and HA hysteresis loops after field annealing samples with $t_{NiO}=5$ and 50 nm for 1 h are displayed in Fig. 9. Both EA loops show a similar behavior as for the nonannealed samples. For $t_{NiO}=5$ nm a slight decrease, for $t_{NiO}=50$ nm a slight increase, in coercivity is observed. $H_{EB,AF}$ has decreased for $t_{NiO}=50$ relative to the as-deposited state. The shape of the HA loops, however, has substantially changed. For the thinner NiO the HA-like loop shape has disappeared [Fig. 9(c)]. Only a weak indication of anisotropy is visible comparing the EA and HA loops. No anisotropy field $H_{EB,AF}$ can be extracted for the thin NiO thickness. At $t_{NiO}=50$ nm a clear HA loop shape is visible.

An overview of the dependence of static and dynamically obtained magnetic properties is given in Fig. 10. Similar dependencies of $H_{EB,AF}$ and $H_{dyn,AF}$ as for the as-deposited films (Fig. 7) are obtained. The value of exchange bias field $H_{EB,AF}$ is somewhat reduced relative to the as-deposited state. Also, the onset of exchange bias $H_{EB,AF}$ is shifted to higher NiO thicknesses relative to the as-deposited state.

As for the as-deposited samples, distinct anisotropy contributions are obtained from the different measurement techniques [Fig. 10(b)]. The values of $H_{stat,AF}$ are much closer to those of $H_{EB,AF}$ and have decreased relative to the as-

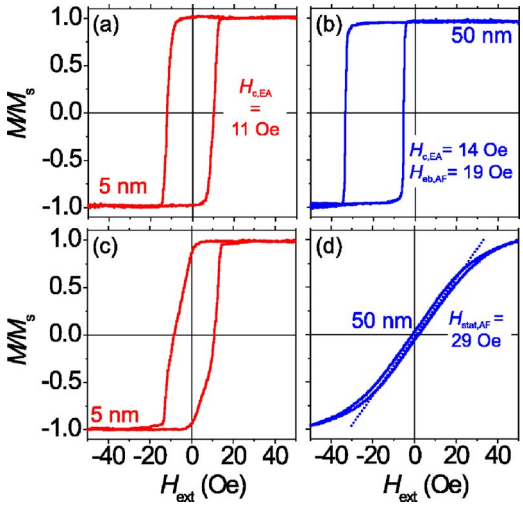

FIG. 9. (Color online) EA hysteresis loops of $Ni_{81}Fe_{19}$ (30 nm)/NiO bilayers with a NiO thickness of (a) 5 and (b) 30 nm. The exchange bias field $H_{EB,AF}$ and the coercivity values $H_{c,EA}$ are indicated. The corresponding HA loops are shown in (c) and (d). The values of $H_{stat,AF}$ for the bilayer samples are shown.

deposited state. The dynamically obtained anisotropy field $H_{dyn,AF}$ peaks at t_{NiO}=5 nm and is then almost constant over a wide NiO thickness range. It has strongly increased from the as-deposited state. No match between $H_{stat,AF}$ and $H_{dyn,AF}$ is found for any NiO thickness. Whereas for the as-deposited state the main contribution to the upward precessional frequency shift was due to a combined uniaxial and cubic anisotropy, after annealing it results from the now predominating rotatable anisotropy field $H_{rot,AF}$ [Fig. 10(b)]. This indicates that the amount of loose AF spins has increased, whereas the contribution of fixed AF spins to the exchange bias stays nearly constant.

Again, the NiO thickness dependence of the nonbiased part of the anisotropy field $H_{k,AF}+H_{rot,AF}$ correlates with the effective damping parameter α_{eff} (Fig. 11). The value of α_{eff}

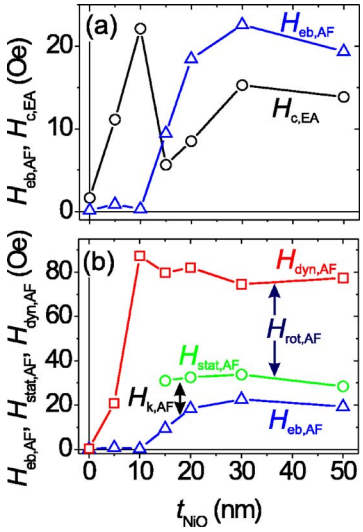

FIG. 10. (Color online) (a) Coercivity $H_{c,EA}$ and exchange bias field $H_{EB,AF}$ as a function of NiO thickness. In (b) $H_{EB,AF}$, $H_{stat,AF}$, and $H_{dyn,AF}$ are compared.

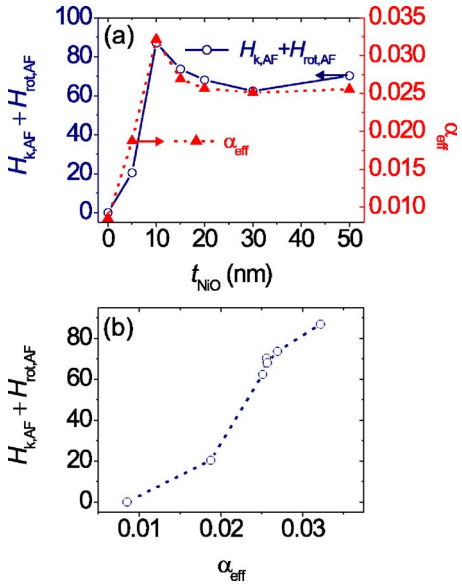

FIG. 11. (Color online) (a) Damping parameter α_{eff} (▲) and $H_{k,AF}+H_{rot}$ (○) as a function of NiO thickness. The correlation between α_{eff} and $H_{k,AF}+H_{rot}$ is plotted in (b).

has increased by a factor of 2 relative to the as-deposited state. This is again in agreement with the assumption of spin-wave damping due to relaxation processes into the AF layer. However, the increase in α_{eff} is higher than for the nonannealed samples. To better understand the change with annealing and the influence of the concurrent formation of a $Ni_xFe_yO_z$ layer at the F/AF interface (see Sec. III), experiments with subsequent short annealing steps were performed.

C. Subsequent annealing

To separate the influence of temperature history and change in interlayer structure, the change of magnetic properties for t_{NiO}=50 nm with subsequent magnetic annealing with a dwell time of 1 min at 250 °C was studied. Magnetization loops recorded after one and after 13 anneals are shown in Fig. 12. After the first annealing cycle, a strong decrease in $H_{EB,AF}$ relative to the as-deposited state occurs. It drops from $H_{EB,AF}$=23 to 12 Oe. A slight increase in coercivity from H_c=8 to 11 Oe takes place. After 13 annealing cycles, $H_{c,EA}$ and $H_{EB,AF}$ have increased. The value of $H_{c,EA}$=20 Oe is higher than after the 1 h anneal, indicating differences in the kinetics of the processes. After several annealing cycles, the exchange bias field $H_{EB,AF}$ becomes comparable to the continuous anneal case, but is still slightly smaller than in the as-deposited state. Noticeably, the increased loop shift is accompanied by an increase in $H_{c,EA}$. Also along the HA the measured anisotropy changes with annealing cycles [Figs. 12(c) and 12(d)]. As in Fig. 9, no obvious signature of a two-step reversal is visible after the first annealing step. Here, the shape of the HA loops can also be modeled by the introduction of additional anisotropy terms similar to Fig. 5(b) (not shown). With further temperature treatments, the amount of static HA anisotropy $H_{stat,AF}$ grows again, which is mainly due to the increase in $H_{EB,AF}$.

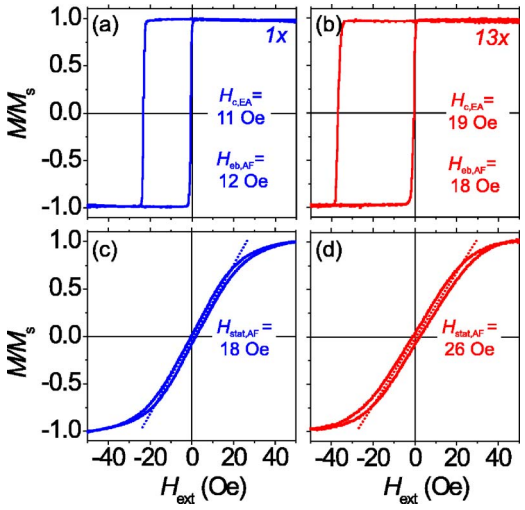

FIG. 12. (Color online) Hysteresis loops along the EA of a $Ni_{81}Fe_{19}$ (30 nm)/NiO (50 nm) bilayer after one (a) and 13 annealing cycles (b) of 1 min dwell time. The corresponding HA loops are shown in (c) and (d). The values of $H_{stat,AF}$ for the bilayer samples are indicated.

An overview of the change of the same magnetic properties as is plotted in Figs. 7 and 10 is given in Fig. 13. As already indicated by the data in Fig. 12, $H_{c,EA}$ constantly increases with annealing cycles. On the other hand, $H_{EB,AF}$ drops initially and then increases with subsequent annealing cycles. In addition, the amount of static HA anisotropy $H_{stat,AF}$ drops significantly after the first anneal. The same increase as for $H_{EB,AF}$ is observed for the static HA anisotropy field $H_{stat,AF}$. The difference between $H_{EB,AF}$ and $H_{stat,AF}$ becomes smaller after the first anneal and stays almost constant from there on. The dynamically obtained $H_{dyn,AF}$ is almost unchanged from the beginning and then increases considerably with annealing cycles. Very similar

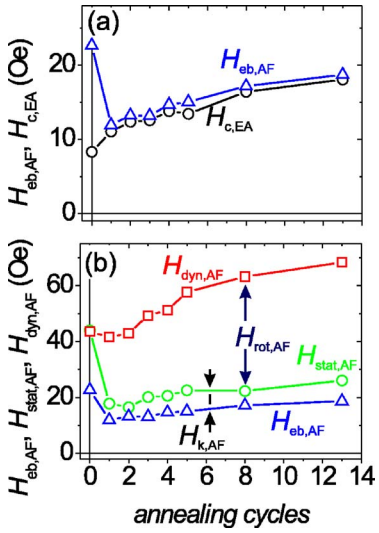

FIG. 13. (Color online) (a) Coercivity $H_{c,EA}$ and exchange bias field $H_{EB,AF}$ as a function of annealing cycles. In (b) the dependences of $H_{EB,AF}$, $H_{stat,AF}$, and $H_{dyn,AF}$ with annealing are compared.

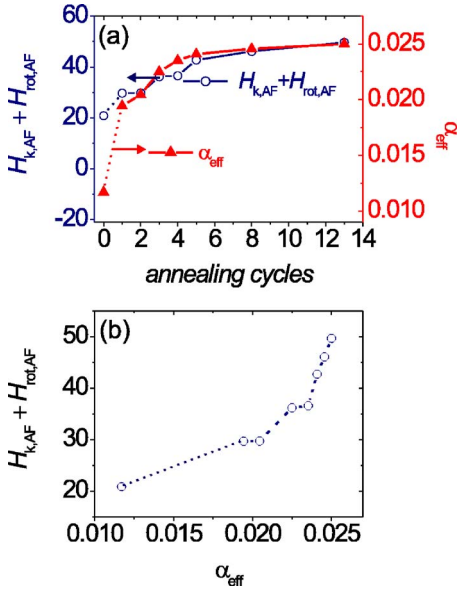

FIG. 14. (Color online) (a) Damping parameter α_{eff} and $H_{k,AF}+H_{rot}$ as a function of annealing steps. The correlation between α_{eff} and $H_{k,AF}+H_{rot}$ is displayed in (b).

dependencies are found at the onset of exchange bias at $t_{NiO}=50$ nm (not shown). The initially unchanged overall anisotropy $H_{dyn,AF}$ together with the drop in $H_{EB,AF}$ indicates a transformation of fixed to movable AF spins, most likely due to a change of the internal AF domain structure resulting from the different magnetic history of the as-deposited film structure. This assumption is in agreement with the observed difference between the statically and dynamically obtained anisotropy field values, which increase from zero to $H_{rot,AF} \approx 22$ Oe after the initial anneal. Noticeably, with subsequent annealing steps, the amount of $H_{dyn,AF}$ increases even further. As already seen for the 1 h annealed samples (Fig. 10), with long annealing times $H_{rot,AF}$ becomes the main contribution to the dynamic anisotropy $H_{dyn,AF}$. While the thermal history of the sample for each anneal is similar, the additional and subsequently occurring changes must occur from the formation of the chemically changed interfacial structure. The ratio between the static and dynamic anisotropy contributions is almost constant after the first annealing steps indicating an increase in overall coupling with annealing.[21]

As for the measurements before, the unfixed anisotropy field $H_{rot,AF}+H_{k,AF}$ scales with the effective damping parameter α_{eff} (Fig. 14). A pronounced step from $\alpha_{eff}=0.013$ to $\alpha_{eff}=0.019$ occurs with the first anneal, which agrees with the assumption of an increase of movable AF spins after the initial heat treatment. The further alteration of damping up to $\alpha_{eff}=0.025$ is related to the changes at the interface. From our data, we cannot distinguish if this change is due to the increase in interfacial coupling, due to a decrease in magnetic homogeneity across the interface, due to enhanced spin-wave damping into the additional $Ni_xFe_yO_z$ layer, or a result of a combination of the above.

V. SUMMARY

In summary, the alterations of static and dynamic anisotropy fields of $Ni_{81}Fe_{19}$/NiO with thermal history and over a

wide range of t_{NiO} thickness were studied. With annealing, a $Ni_xFe_yO_z$ layer forms at the F/AF interface.

Without the existence of in-plane texture, four different anisotropy contributions are identified from the static and dynamic measurements. Remarkably, the overall coupling or exchange anisotropy is constant over a wide range of NiO thickness, independent of the occurrence of exchange bias. This indicates the same origin for all the observed higher-order anisotropy terms. Only for very thin NiO layer thickness in combination with annealing, a reduction in overall anisotropy was found (Fig. 10). This is attributed to a reduction of the effective thickness of the AF layer due to the interlayer mixing derived from analytical TEM. The reduction of effective AF thickness also manifests itself in a shift of the onset of $H_{eb,AF}$ (comparing Figs. 7 and 10) for the as-deposited and 1 h annealed case, respectively. For all thicknesses above $t_{NiO}=5$ nm, the total dynamic anisotropy $H_{dyn,AF}$ is nearly constant and only changes with thermal history.

The amount of rotatable anisotropy and the effective magnetic damping parameter correlate directly with the nonunidirectional parts of AF anisotropy and the stability of the AF spin structure, respectively. The interpretation of the data indicates that the spin structure inside the antiferromagnetic layer determines the amount of exchange bias and is the dominating contribution to coercivity, as seen from the AF thickness dependence. The interfacial structure itself is mostly important for the overall exchange anisotropy.

Some of the results presented here can be described in the framework of the model of Stiles and McMichael.[32] However, as for most publications on exchange bias, other models may also apply to explain the experimental data. Nevertheless, neither of the so far published theories includes changes with thermal history, which alters the AF domain structure, nor the formation of a third magnetic layer at the interface. As shown, to achieve an understanding of the exchange bias phenomenon in polycrystalline samples, the real microstructure and the thermomagnetic history have to be considered.

ACKNOWLEDGMENTS

The authors would like to thank J. Dshemuchadse for providing the code for the hysteresis modeling. Additional thanks go to R. Schäfer for carefully reading the manuscript and his always helpful suggestions.

*Electronic address: j.mccord@ifw-dresden.de

[1] W. H. Meiklejohn and C. P. Bean, Phys. Rev. **102**, 1413 (1956).
[2] A. Berkowitz and K. Takano, J. Magn. Magn. Mater. **200**, 552 (1999).
[3] J. Nogues and I. K. Schuller, J. Magn. Magn. Mater. **192**, 203 (1999).
[4] R. L. Stamps, J. Phys. D **33**, R247 (2000).
[5] D. Mauri, H. C. Siegmann, P. S. Bagus, and E. Kay, J. Appl. Phys. **62**, 3047 (1987).
[6] A. P. Malozemoff, J. Appl. Phys. **63**, 3874 (1988).
[7] K. Takano, R. H. Kodama, A. E. Berkowitz, W. Cao, and G. Thomas, Phys. Rev. Lett. **79**, 1130 (1997).
[8] M. D. Stiles and R. D. McMichael, Phys. Rev. B **63**, 064405 (2001).
[9] N. C. Koon, Phys. Rev. Lett. **78**, 4865 (1996).
[10] U. Nowak, A. Misra, and K. D. Usadel, J. Appl. Phys. **89**, 7269 (2001).
[11] D. Suess, M. Kirschner, T. Schrefl, J. Fidler, R. L. Stamps, and J. V. Kim, Phys. Rev. B **67**, 054419 (2003).
[12] H. Ohldag, A. Scholl, F. Nolting, E. Arenholz, S. Maat, A. T. Young, M. Carey, and J. Stohr, Phys. Rev. Lett. **91**, 017203 (2003).
[13] A. Scholl, M. Liberati, E. Arenholz, H. Ohldag, and J. Stohr, Phys. Rev. Lett. **92**, 247201 (2004).
[14] T. Zhao, H. Fujiwara, K. Zhang, C. Hou, and T. Kai, Phys. Rev. B **65**, 014431 (2001).
[15] T. Ambrose, R. L. Sommer, and C. L. Chien, Phys. Rev. B **56**, 83 (1997).
[16] C. Leighton, M. R. Fitzsimmons, P. Yashar, A. Hoffmann, J. Nogues, J. Dura, C. F. Majkrzak, and I. K. Schuller, Phys. Rev. Lett. **86**, 4394 (2001).
[17] E. Fulcomer and S. H. Charap, J. Appl. Phys. **43**, 4190 (1972).
[18] C. Leighton, J. Nogues, B. J. Josson-Akerman, and I. K. Schuller, Phys. Rev. Lett. **84**, 3466 (2000).
[19] H. Xi and R. M. White, Phys. Rev. B **61**, 80 (2000).
[20] C. Schlenker, S. Parkin, J. Scott, and K. Howard, J. Magn. Magn. Mater. **54-57**, 801 (1986).
[21] H. Ohldag, T. J. Regan, J. Stohr, A. Scholl, F. Nolting, J. Luning, C. Stamm, S. Anders, and R. L. White, Phys. Rev. Lett. **87**, 247201 (2001).
[22] R. D. McMichael, M. D. Stiles, P. J. Chen, and W. F. Egelhoff, Phys. Rev. B **58**, 8605 (1998).
[23] P. Miltnyi, M. Gruyters, G. Guntherodt, J. Nogues, and I. K. Schuller, Phys. Rev. B **59**, 3333 (1999).
[24] S. M. Rezende, A. Azevedo, M. A. Lucena, and F. M. deAguiar, Phys. Rev. B **63**, 214418 (2001).
[25] J. McCord, R. Mattheis, and D. Elefant, Phys. Rev. B **70**, 094420 (2004).
[26] R. Arias and D. L. Mills, Phys. Rev. B **60**, 7395 (1999).
[27] R. D. McMichael, C. G. Lee, M. D. Stiles, F. G. Serpa, and P. J. Chen, J. Appl. Phys. **87**, 6406 (2000).
[28] R. J. Prosen, J. O. Holmen, and B. E. Gran, J. Appl. Phys. **32**, S91 (1961).
[29] T. J. Silva, C. S. Lee, T. M. Crawford, and C. T. Rogers, J. Appl. Phys. **85**, 7849 (1999).
[30] C. Kittel, Phys. Rev. **73**, 155 (1948).
[31] G. Sandler, H. Bertram, T. J. Siva, and T. Crawford, J. Appl. Phys. **85**, 5080 (1999).
[32] M. D. Stiles and R. D. McMichael, Phys. Rev. B **59**, 3722 (1999).
[33] H. Xi, R. White, and S. Rezende, Phys. Rev. B **60**, 14837 (1999).
[34] B. Kuanr, R. Camley, and Z. Celinski, J. Appl. Phys. **93**, 7723 (2003).